Polyacrylamide Adsorption from Aqueous Solutions on Gold and Silver Surfaces Monitored by the Quartz Crystal Microbalance

Jeffrey C. Munro and Curtis W. Frank*

Department of Chemical Engineering, Stanford University, Stanford, California 94305-5025

Received May 30, 2003

ABSTRACT: Viscoelastic properties of ultrathin films are important in such applications as polymer-supported lipid bilayers, and the quartz crystal microbalance (QCM) offers the ability to measure these properties in situ. In this study, polymer films are created by adsorbing polyacrylamide to gold and silver surfaces from aqueous solutions. The molecular weight of the polymers ranges from 10 000 to 1 000 000 g/mol, and concentrations range from dilute to the overlap concentration. Using a continuum mechanics viscoelastic film model, we extract film property parameters from frequency and dissipation change measurements for multiple harmonics. The precision of the QCM and the modeling technique are limited, however, leading to large property value ranges for any given film. The adsorbed films range from 10 to 150 Å thick, with moduli ranging from 15 to 228 kPa and viscosities ranging from 1.21×10^{-3} to 2.85×10^{-3} Pa s. Meanwhile, the bulk solution properties of the different molecular weight materials lead to drastically different adsorption profiles. While the viscosity differences between water and 10 000 M_w polymer solutions lead to large frequency and dissipation responses, the large relaxation times of 1 000 000 M_w polymers make their bulk solution viscosity differences from water largely undetectable by the QCM. In addition, the viscosity of the 10 000 M_w solutions may be frequency dependent over the range of operating frequencies, contrary to the standard QCM assumption of frequency independence.

Introduction

Various lipid bilayer systems have been used to study the structure and function of biomembranes.[1] Perhaps the simplest and most commonly studied bilayer systems are solid-supported lipid bilayers formed on hydrophilic glass. These bilayers show good fluidity due to the presence of a thin (10−20 Å) lubricating layer of water between the bilayer and the substrate.[2−4] However, large transmembrane proteins inserted into solid-supported bilayer systems often lose their lateral mobility due to protein domains extending beyond the confines of the bilayer and making contact with the solid substrate.[5−7] To create a large enough separation between the lipid bilayer and solid substrate to allow protein mobility, many authors have suggested introducing a soft, deformable hydrophilic polymer cushion as a spacer.[8]

Numerous designs have been proposed for such polymer-supported lipid bilayer systems. Bilayers have been supported on thin films of polymers such as polyethylenimine,[9−12] polyacrylamide,[13] agarose,[14] and dextran.[15] More complicated systems that provide covalent bonding of the polymer to the solid substrate as well as anchoring of the polymer support to the lipid bilayer have also been constructed.[16−18] We reported previously on the adsorption behavior and viscoelastic properties of random copolymers consisting of an acrylamide backbone with lipid side chains and disulfide-containing side chains.[19] In this study, we quantify the thicknesses of adsorbed polyacrylamide (PA) films and their properties as a function of molecular weight and concentration on two metallic surfaces, silver and gold, using a quartz crystal microbalance with dissipation (QCM-D).

There have been few studies on the adsorption of PA to gold and silver surfaces. Grchev et al. studied the adsorption of PA on gold using cyclic voltammetry and capacity measurements.[20,21] Using PAs with molecular weights ranging from 5000 to 1 600 000 g/mol at ppm concentrations, they observed complete coverage and layer thicknesses of about 10 Å. Grchev et al. concluded that PA adsorbs very tightly to gold, resulting in flat conformations of adsorbed molecules. PA adsorption to silica has also been studied, but the interactions between PA and the silica surface were largely due to hydrogen bonding, which is much different from the types of interactions expected for metal surfaces.[22]

Several other methods have been used to study polymer adsorption on planar surfaces, including radiolabeling,[23] reflectance FTIR,[24] in situ ellipsometry,[25] and in situ surface plasmon resonance.[26] However, the mechanical oscillatory nature of the QCM offers the ability to measure in situ viscoelastic properties of thin polymer films in addition to the mass uptake. Initially, QCM was used in a vacuum or air solely to measure the mass of rigid films adsorbed to the quartz crystal.[27] The well-known Sauerbrey equation states that the resonance frequency change of the quartz crystal, Δf, is directly proportional to the adsorbed mass.[28] In 1980, Nomura and Minemura established that the QCM could also function in liquids.[29] That discovery has prompted a vast number of experimental and theoretical treatments of the quartz resonator operating in lossy media, including viscous liquids, viscoelastic films, or combinations of the two. Buttry and Ward provide an early review.[30]

An important feature of QCM work involving lossy materials is the determination of a second parameter in addition to Δf. Three methods are commonly used to obtain QCM parameters. Steady-state methods include compensated phase-locked oscillation and impedance analysis. In the former, a compensated phase-locked oscillator provides a frequency and equivalent circuit resistance. In the latter, impedance analysis yields the

* To whom correspondence should be addressed: e-mail curt.frank@stanford.edu.

10.1021/ma030297w CCC: $27.50
Published on Web 01/15/2004

frequency as well as either equivalent circuit parameters (resistance, capacitance, and inductance) or the resonance peak bandwidth, which can be related to the *Q*-factor. More recently, a transient method has been developed where the frequency and transient decay time are measured.[31] The decay time, equivalent circuit parameters, *Q*-factor, and dissipation change, ΔD, can all be related to each other and provide comparable information. A recent review by Geelhood et al. compares the three methods for obtaining QCM parameters.[32] In this study, we use the QCM-D method to collect Δf and ΔD data.

To extract useful information from QCM data, Δf and ΔD have to be related to material properties. Two early examples of such relationships for Δf are the Sauerbrey equation, which relates film thickness and density to Δf, and a bulk Newtonian fluid equation derived by Kanazawa and Gordon, which relates the density−viscosity product of the fluid to Δf.[33,34] Unfortunately, when viscoelastic films or liquids are introduced, the relationships between material properties and Δf and ΔD become more complex. For example, viscoelastic films may be described by four parameters—thickness, density, and two shear modulus components (storage and loss moduli). Since the QCM can only provide two experimental observables at a given frequency, a unique fit for all four film parameters cannot be obtained.

While several authors have considered various combinations of viscoelastic layers on quartz resonators,[35−41] few have successfully extracted viscoelastic film properties from QCM data.[42−45] Several approaches have been used to reduce the problem to two fitting parameters. Hillman et al. provide a brief review of the most commonly employed strategies.[45] One successful strategy first uses simultaneous QCM and electrochemistry measurements of thin, lossless films to determine film density, which is then assumed to remain constant for thicker films.[45] Then, while electrochemistry measurements of thick films provide the thickness, QCM impedance measurements of the same films are used to obtain the storage and loss moduli. In general, any technique that can provide independent values for two film parameters would allow a unique fit of the other two parameters using QCM data.

Material properties have also been determined for relatively thick films, on the order of hundreds of nanometers thick, using QCM measurements at multiple frequencies.[42,46] Such thick films often have film resonances, which make the determination of film properties relatively straightforward. In this study, we use Δf and ΔD data collected at multiple harmonics to determine the viscoelastic properties of adsorbed PA thin films surrounded by a bulk liquid. We model the viscoelastic films using a Voigt model, which imposes a specific frequency dependence on the storage and loss moduli such that only two input parameters are required to describe the viscoelasticity of the system over the 5−35 MHz operating frequency range of the QCM. We discuss the film properties in terms of film structure as well as the contribution of the bulk polymer solution to Δf and ΔD as a function of molecular weight.

Experimental Section

Materials. Three different molecular weight PA samples were used. 10 000 M_w PA (unknown polydispersity) was obtained from Aldrich (Sigma-Aldrich Corp., Milwaukee, WI) as a 50 wt % solution in water. 500 000 and 1 000 000 M_w PAs (polydispersities ~ 2.5) were obtained from Polysciences (Polysciences, Inc., Warrington, PA) as powders. Polymer solutions at five concentrations (c^*, $c^*/3$, $c^*/6$, $c^*/30$, and $c^*/300$, where c^* is the overlap concentration) were prepared using Milli-Q water (18.2 MΩ, Millipore Corp., Bedford, MA). Overlap concentrations were estimated as follows:

$$c^* \approx \frac{1}{[\eta]} = \frac{1}{KM_v{}^a} \tag{1}$$

where $[\eta]$ is the intrinsic viscosity, M_v is the viscosity-average molecular weight (approximated as the weight-average molecular weight, M_w), and K and a are the Mark−Houwink fitting parameters.[47] The estimated values of c^* were 52.9, 5.0, and 3.1 mg/mL for 10 000, 500 000, and 1 000 000 M_w PAs, respectively. All polymers were soluble with minimal stirring, but solutions were allowed to equilibrate for at least 24 h before use. The viscosities of the polymer solutions were determined at 25.0 ± 0.5 °C using a Ubbelohde viscometer. An average of three runs for each solution was obtained. To determine the experimental viscosity from the relative viscosity, we used a viscosity of 8.9×10^{-4} Pa s for water at 25 °C.[48]

Ellipsometry. Dry thicknesses of adsorbed PA films on silver were determined with a Gaertner L116C ellipsometer (Gaertner Scientific Corp., Chicago, IL) equipped with a He−Ne laser (λ = 6328 Å) at an incident angle of 70°, assuming an index of refraction of 1.46. Substrates consisted of silicon wafers coated in an Edwards Auto 306 evaporator (BOC Edwards, West Sussex, UK) with approximately 3 nm chromium and 100 nm of silver (99.99%, Plasmaterials, Livermore, CA). Substrates were removed from the evaporator and placed directly in aqueous polymer solutions for approximately 2 h. Following adsorption, each sample was removed from the polymer solution, rinsed with water, and dried under a stream of N_2. Measurements were taken at four different locations on each sample and averaged.

Quartz Crystal Microbalance with Dissipation. QCM-D was conducted on a Q-Sense D300 (Q-Sense AB, Gothenburg, Sweden) fitted with a QAFC 301 axial flow chamber. The QCM-D technique is described elsewhere.[49] In summary, a quartz crystal is driven at its resonance frequency of 5 MHz or at one of its first three overtones: 15, 25, or 35 MHz. Then, the drive circuit is short-circuited, and the exponential decay of the oscillation amplitude is monitored. The dissipation is obtained from the single-exponential decay constant that describes the decaying oscillation amplitude. AT-cut quartz crystals 14 mm in diameter and coated with a few nanometers titanium as an adhesion layer and about 100 nm of gold were purchased from Q-Sense. For measurements on gold, the quartz crystals were cleaned with oxygen plasma (1 Torr, 75 W) for 2 min (March Plasmod Plasma Etcher, March Instruments, Inc., Concord, CA), soaked in ethanol (200 proof) for 10 min, and dried under a stream of N_2, as suggested by Ron et al.[50] For measurements on silver, the front-side electrode of the gold-coated quartz crystal was coated with approximately 50 nm of silver in an Edwards Auto 306 evaporator. For reuse, silver-coated crystals were dipped in concentrated nitric acid for about 5 s to remove the silver, rinsed thoroughly with water, and then recoated with fresh silver. All measurements were conducted at 25.0 ± 0.03 °C. Δf and ΔD values were obtained at the fundamental frequency (5 MHz) and three overtones (15, 25, and 35 MHz), with Milli-Q water used for the baseline. After equilibrating the QCM-D chamber in water, approximately 0.5 mL of polymer solution was rinsed through the measurement chamber, which has a volume of approximately 0.1 mL, over approximately 2 min. After a 2 h adsorption period, the chamber was rinsed with about 0.5 mL of water over about 2 min. QCM-D data were modeled with a commercial software package, QTools, provided by Q-Sense, as described in the Modeling Results QCM-D Model section below.

Rheology. The shear-rate-dependent viscosity of PA solutions was measured with a Rheometric Scientific ARES rheometer (Rheometric Scientific, Inc., Piscataway, NJ) using a 50 mm cone and plate geometry. Note that a quartz crystal

Table 1. PA Film Properties

PA M_w/ surface	concn	water-swollen, viscoelastic film: modulus, μ_F (kPa)	viscosity, η_F (mPa s)	thickness, t_F (Å)	ellipsometry: dry film thickness (Å)
10 000/Au	*c**/300	502	2.65	16	
	*c**/30	384	1.17	13	
	*c**/6	112	1.70	54	
	*c**/3	111	1.60	64	
	*c**	59	1.49	73	
10 000/Ag	*c**/300	65	1.92	37	9
	*c**/30	99	1.68	45	14
	*c**/6	87	1.58	67	16
	*c**/3	57	1.58	77	17
	*c**	66	1.51	74	17
1 000 000/Ag	*c**/300	86	1.10	6	9
	*c**/30	258	2.68	15	11
	*c**/6	60	1.53	48	12
	*c**/3	155	1.65	52	17
	*c**	61	1.45	147	16

resonates in a small-amplitude oscillatory shear motion. Unfortunately, the maximum frequency available for a small-amplitude oscillatory shear experiment on the rheometer was only 100 Hz, almost 5 orders of magnitude less than the operating frequency of the QCM. Therefore, we chose to use the steady-shear mode of the rheometer, where a maximum shear rate of approximately 4000 s^{-1} was possible. Solutions of 10 000 M_w and 1 000 000 M_w PAs were prepared at *c** concentrations in 85/15 wt % mixtures of glycerol/water. The glycerol/water mixture was used in order to increase the viscosity of the solvent phase. The polymer samples showed good solubility after stirring for 24 h. The shear-rate-dependent viscosity was measured at 24.8 ± 0.2 °C using a steady shear-rate test in a strain-controlled mode. The shear rate was held constant for 10 s, with the last 5 s used for the measurement.

Experimental Results

Ellipsometry. To obtain polymer film data independent of that derived from the QCM-D modeling, ellipsometry was used to determine dry PA film thicknesses. The thickness values are presented in Table 1 along with the film parameters from the viscoelastic film model fits discussed below. The dry film thicknesses are significantly less than the values from the model fits. However, the films in situ are likely to be quite different from dry films. PA is a highly hydrophilic polymer and likely to be quite swollen in the aqueous environment, unlike the dry films that are quite likely to be completely collapsed.

Quartz Crystal Microbalance with Dissipation. Adsorption profiles for 10 000 and 1 000 000 M_w PAs at each concentration on silver are shown in Figures 1 and 2. Δf and ΔD at 15 MHz are shown with water as the baseline. The small Δf and ΔD changes near 130 min are due to a temperature change in the chamber. The chamber is maintained at 25.0 °C, but when liquid at room temperature (~20 °C) is exchanged in the small warm-up loop in the QCM-D chamber, the load on the heating element changes, causing a small temperature change. In general, it takes 3−4 min for Δf and ΔD to recover.

As shown in Figures 1 and 2, the magnitudes of Δf and ΔD increase with increasing concentration. However, clear differences appear in the adsorption profiles for the different molecular weights. For the 10 000 M_w samples, large changes in Δf and ΔD result immediately after adding polymer solution, followed by only minor changes over the remainder of the adsorption time. This is particularly true for ΔD. With the exception of the *c**/300 solution, significant changes in Δf and ΔD take

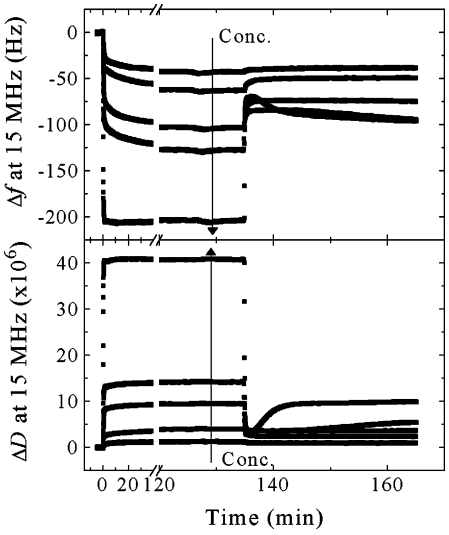

Figure 1. QCM-D data (Δf and ΔD) at 15 MHz for 10 000 M_w PA on silver. The baseline corresponds to water in the measurement chamber. Polymer solution flows through the cell at 0 min, and water is rinsed through the cell at approximately 135 min. The five curves correspond to the following five concentrations *c**, *c**/3, *c**/6, *c**/30, and *c**/300, where the arrow points in the direction of increasing concentration. Polymer solutions were tested twice; these are representative data sets. Variation from run to run was up to ±10%.

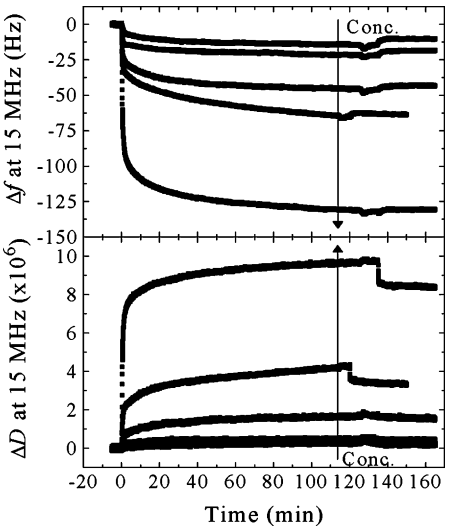

Figure 2. QCM-D data (Δf and ΔD) at 15 MHz for 1 000 000 M_w PA on silver. Conditions are identical to Figure 1.

place when water is exchanged for the polymer solution. For the highest concentrations, apparent overshoots in Δf and ΔD occur with the 0.5 mL water rinse. In the adsorption profile of a 10/90 wt % glycerol/water mixture, whose viscosity is similar to the *c** PA solutions, a similar overshoot is observed after one rinse (see Figure 3). In that experiment, Δf and ΔD initially return to baseline values, as expected for complete bulk fluid exchange. Then Δf and ΔD increase in magnitude. However, if a second rinse of 0.5 mL of water is performed in the glycerol/water experiment, there is no overshoot; Δf and ΔD return to baseline values and remain constant. Thus, we believe that the overshoots observed for the higher concentration polymer solutions result from insufficient exchange of water for polymer solution provided by the single rinse of 0.5 mL of water. This is only observable when a large difference exists between the viscosity of the polymer solution and that

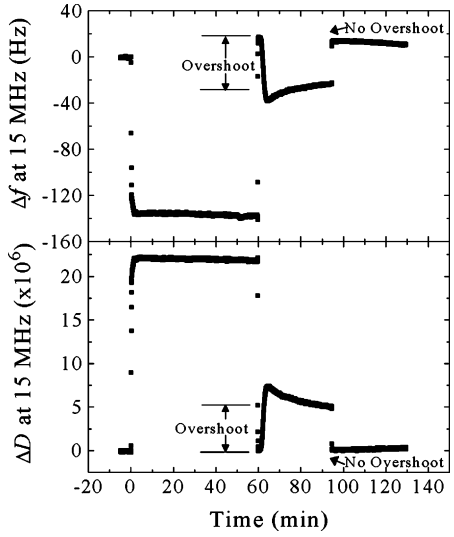

Figure 3. QCM-D data (Δf and ΔD) at 15 MHz for 10/90 wt % glycerol/water mixture on silver. The baseline corresponds to water in the measurement chamber. A glycerol/water mixture flows through the cell at 0 min, and water is rinsed through the cell at approximately 60 and 95 min.

of water. While a second rinse of 0.5 mL of water was not performed, we believe accurate postrinse Δf and ΔD values for solutions with an overshoot can be obtained by using values immediately after the rinse, where the Δf and ΔD magnitudes are at a minimum. These Δf and ΔD values should represent a well-rinsed system, as was the case in the glycerol/water experiment.

For the 1 000 000 M_w PA on silver, the magnitudes of Δf and ΔD before the water rinse are much smaller than for the 10 000 M_w materials. In addition, significant Δf and ΔD changes take place over the 2 h adsorption profile even after the initial jump at 0 min, as can be seen by the rounded shape of the adsorption profiles. At the rinsing step, there are no changes in Δf and only small changes in ΔD for the two highest concentrations. As a result, Δf and ΔD values are larger for the 1 000 000 M_w materials after the water rinse than for the 10 000 M_w materials. Results for the 500 000 M_w PA on silver are similar to the 1 000 000 M_w results and are not shown.

To determine whether the character of the metal surface influences the PA adsorption behavior, adsorption profiles for 10 000 M_w PA on gold were collected. Since the adsorption profiles for the 10 000 M_w samples on gold have very similar shapes to those seen on silver, the data are not shown. In addition, because the character of the surface seemed to have only a small effect on the adsorption profiles, data were not collected for other molecular weights on gold.

Rheology. Many aqueous polymer solutions show non-Newtonian shear-thinning behavior.[51,52] Therefore, it is possible that the viscosities measured with the Ubbelohde viscometer are not accurate representations of the viscosity of the fluid sensed by the QCM, which operates at a very high frequency. To determine the shear-thinning properties of these PA solutions, we determined the shear-rate-dependent viscosity of c^* solutions of 10 000 and 1 000 000 M_w PA in glycerol/water mixtures. Figure 4 shows the shear-rate dependent viscosity of the solutions tested. Even though glycerol/water mixtures are reported to be Newtonian fluids over the shear rates tested, Figure 4 shows that the viscosity of the 85/15 glycerol/water mixture drifts

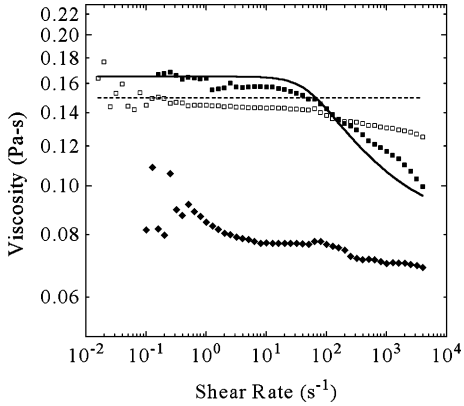

Figure 4. Shear-thinning of c^* PA glycerol/water solutions: (◆) 85/15 wt % glycerol/water, (□) 10 000 M_w c^* PA, and (■) 1 000 000 M_w c^* PA. Theoretical curves, (---) 10 000 M_w and (—) 1 000 000 M_w, are based on the Carreau and Rouse models, as discussed in the text.

to lower values at higher shear rates.[53] The 10 000 M_w PA solution shows a similar behavior with only a small decrease in viscosity at higher shear rates. Meanwhile, the 1 000 000 M_w PA solution shows clear shear thinning behavior above 50 s^{-1}.

The Carreau model[52] is often used to describe shear-thinning behavior:

$$\eta(\dot{\gamma}) = \eta_\infty + \frac{\eta_0 - \eta_\infty}{[1 + (\tau\dot{\gamma})^2]^{p/2}} \qquad (2)$$

where $\dot{\gamma}$ is the shear rate, η_∞ is the viscosity at infinite shear rate (estimated as the viscosity of the solvent), η_0 is the zero-shear rate viscosity, τ is a fitting parameter that describes the characteristic time scale, and p is a fitting parameter that describes how quickly the viscosity decreases. Theoretical curves that follow the Carreau model are also shown in Figure 4. The average of the viscosity values over all shear rates for 85/15 wt % glycerol/water mixture is used for η_∞. The viscosities of each solution at low shear rates (below 10 s^{-1}) are averaged to provide η_0. The parameter p is taken from the literature. López et al. performed similar steady shear-rate tests on a 12 000 000 M_w PA in 85/15 wt % glycerol/water solutions at several concentrations.[52] Because p ranged from 0.30 to 0.42 in their experiments, we used the average value of $p = 0.37$ here. The characteristic time, τ, can be estimated from the Rouse model, which gives the longest relaxation time, τ_1:

$$\tau_1 = 0.608\frac{(\eta_0 - \eta_\infty)M_w}{cRT} \qquad (3)$$

where c is the mass concentration of the polymer solution, R is the gas constant, and T is the temperature. In previous studies, where τ is determined by fitting viscosity data to the Carreau model, it has been found that values of τ are approximately 3 times greater than values of τ_1.[51,52] Therefore, we used the estimation $\tau \cong 3\tau_1$ in the theoretical curves. As shown in Figure 4, the theoretical curve matches the 1 000 000 M_w PA data quite well. On the other hand, the viscosity of the 10 000 M_w solution decreases at higher shear rates, but this is not reproduced by the theoretical curve. However, this decrease in viscosity is approximately the same for that of the Newtonian 85/15 wt % glycerol/water mixture,

suggesting the presence of similar experimental drifts for both of those runs.

Modeling Results

Rather than modeling entire adsorption profiles, two time points on each profile were chosen for the analysis. Prerinse values refer to the average of Δf and ΔD from 119.5 to 120.5 min (approximately 30 values), when there is an adsorbed film and polymer solution present in the chamber. Postrinse values refer to the average of Δf and ΔD from 149.5 to 150.5 min, with the exception of profiles that show an overshoot (10 000 M_w PA c^* on gold and silver and $c^*/3$ on silver), when there is an adsorbed film and water present in the chamber. For these three cases, Δf and ΔD values immediately after the rinse (around 137 min), where the Δf and ΔD magnitudes are at a minimum, are used. Values at all four harmonics were used when possible. (For some of the experimental runs, especially at lower concentrations where the magnitudes of Δf and ΔD were smaller, the data at 5 MHz were unusually noisy and therefore not used. The small size of the quartz crystals used can lead to poor energy trapping at the fundamental frequency, resulting in noise in the data acquisition.[54]) The model results (parameter values) shown and discussed below are averages of values obtained for each profile at a particular concentration and molecular weight.

Scaling of Δf and ΔD with Harmonic Number. Multiple processes may lead to the Δf and ΔD values observed for these PA solutions. First, the bulk fluid surrounding the quartz resonator changes from water to a polymer solution and back to water. Because there is a difference in the viscosity of water and that of the polymer solutions, we must consider the effect of the bulk liquid on Δf and ΔD. Kanazawa and Gordon derived the frequency response to a Newtonian liquid:

$$\Delta f = n^{1/2} f_1^{3/2} (\eta_L \rho_L / \pi \mu_Q \rho_Q)^{1/2} \quad (4)$$

where f_1 is the fundamental frequency, η_L and ρ_L are the viscosity and density of the liquid, $\rho_Q = 2650$ kg/m^3 is the density of the quartz, $\mu_Q = 2.947 \times 10^{10}$ kg m^{-1} s^{-2} is the shear modulus of quartz, and n is the harmonic number, which is the number of half-wavelengths of the thickness shear waves in the crystal.[33] Similarly, ΔD for Newtonian liquids was derived:[55,56]

$$\Delta D = 2(f_1/n)^{1/2} (\eta_L \rho_L / \pi \mu_Q \rho_Q)^{1/2} \quad (5)$$

Second, there may be adsorption of the polymer to the surface resulting in a film. The exchange of water for polymer solution occurs between 0 and 2 min. Referring to Figure 2, we see that changes in Δf and ΔD continue long after this exchange of liquids, suggesting that something in addition to bulk liquid viscosity changes is occurring, namely adsorption of the polymer to the surface. Thus, the effects of a film on Δf and ΔD must also be considered. The classical Sauerbrey equation

$$\Delta f_n = -n \left(\frac{2\rho_F f_n^2}{\rho_Q v_Q} \right) t_F \quad (6)$$

describes how the adsorption of a thin, rigid film on the quartz resonator will lead to a change in frequency. Here, t_F is the film thickness, f_n is the resonance frequency of the crystal with no film at the nth harmonic, ρ_F is the density of the film, and $v_Q = 3340$ m/s is the shear velocity in quartz.[28] The Sauerbrey equation assumes that the adsorbed film is of uniform thickness, is rigid, and obeys no-slip conditions at the interface between the crystal and film. These assumptions correspond to a loss-less film where $\Delta D = 0$.

Table 2. Scaling of Δf and ΔD with Harmonic Number[a]

PA M_w/ surface	concn	α		β	
		prerinse[b]	postrinse[c]	prerinse[b]	postrinse[c]
10 000/Au	$c^*/300$	1.00	1.02	0.14[d]	0.30[d]
	$c^*/30$	0.83	0.97	−0.50	0.21[d]
	$c^*/6$	0.47	0.81	−0.56	−0.10
	$c^*/3$	0.40	0.69	−0.66	−0.07
	c^*	0.40	0.61	−0.65	−0.39
10 000/Ag	$c^*/300$	0.91	0.94	−0.16	−0.09
	$c^*/30$	0.87	1.07	−0.30	−0.14
	$c^*/6$	0.51	0.59	−0.61	−0.35
	$c^*/3$	0.61	0.75	−0.55	−0.39
	c^*	0.33	0.57	−0.59	−0.27
1 000 000/Ag	$c^*/300$	0.09[d]	−0.20[d]	0.60[d]	0.28[d]
	$c^*/30$	0.84	0.83	−0.33	−0.32
	$c^*/6$	0.87	0.84	−0.38	−0.37
	$c^*/3$	0.63	0.63	−0.37	−0.31
	c^*	0.75	0.77	−0.42	−0.29

[a] $\Delta f \sim n^{\alpha}$, $\Delta D \sim n^{\beta}$. [b] Prerinse refers to data at 120 min, before the water rinse. [c] Postrinse refers to 150 min, after the water rinse, except for 10 000 M_w c^* on gold and silver and 10 000 M_w $c^*/3$ on silver where overshoots were apparent. In those cases, postrinse numbers were taken from point after the rinse where Δf and ΔD are at the lowest magnitude. [d] Magnitudes too small to get reliable scaling values.

As seen in eqs 4 and 6, $\Delta f \sim n^{0.5}$ for a Newtonian liquid, but $\Delta f \sim n$ for a solid film. In addition, eq 5 shows that $\Delta D \sim n^{-0.5}$ for a Newtonian liquid. Experimentally, $\Delta f \sim n^{\alpha}$ and $\Delta D \sim n^{\beta}$. By comparing values of α and β with the theoretical scaling values, we can determine whether Δf and ΔD are dominated by bulk Newtonian liquid or rigid film effects. Differences from the theoretical values could indicate a superposition of liquid and rigid film effects or the presence of viscoelastic film effects. For each experiment, pre- and postrinse Δf and ΔD values were plotted against the harmonic number on a log−log plot. The slopes of the fitted lines are used as the experimental scaling values, α and β, as reported in Table 2. Note that at the lower concentrations the magnitudes of Δf and ΔD are small, making the scaling values unreliable.

The 10 000 M_w PAs show solidlike Δf scaling ($\Delta f \sim n^1$) at lower concentrations ($c^*/300$ and $c^*/30$) before and after the rinse. At higher concentrations and prerinse, the α values are closer to liquid values ($\Delta f \sim n^{0.5}$). The increase in the α values from pre- to postrinse indicates a greater solid contribution after the rinse. This is consistent, since after the rinse, the effect of the bulk polymer solution should not be present. For the 1 000 000 M_w PAs, all of the α values lie between liquidlike and solidlike. In addition, there is little change from pre- to postrinse, indicating little change in the factors contributing to Δf.

As with the α values, the β values for the 1 000 000 M_w PAs pre- and postrinse are consistent with a state intermediate between a Newtonian liquid and a rigid solid. Meanwhile, the β values suggest a liquidlike system ($\Delta D \sim n^{-0.5}$) for the 10 000 M_w solutions before the rinse, inconsistent with the α values for the lower concentrations. After the rinse, the β values decrease in magnitude, indicating the loss of the liquid contribution, complementing the Δf scaling changes.

α and β values that are intermediate between liquidlike and solidlike, discrepancies between Δf and ΔD

scaling values for 10 000 M_w solutions, and the shapes of the adsorption profiles all suggest that both the bulk polymer solution and the adsorbed film contribute to Δf and ΔD. In addition, the postrinse α values and nonzero postrinse ΔD values indicate that the films are nonrigid and may not follow the Sauerbrey equation. Ultimately, we must conclude that the simple equations (eqs 4−6) presented above are insufficient to interpret the data correctly. Instead, more complicated theories for viscoelastic films in bulk fluids must be used.

QCM-D Model. The logic we have used to approach this modeling problem is displayed schematically in Figure 5. We attempt to limit the complexity of the model by adding one fitting parameter at a time until a good and physically reasonable solution is found. To extract viscoelastic film properties from the QCM-D data, we use the results of a continuum mechanics analysis, which is described in detail elsewhere.[57,58] In summary, the approach models viscoelastic films as single Voigt or Maxwell elements and the bulk liquid as a Newtonian fluid. A general solution to a wave equation describing the dynamics of the layered system is found, and the crystal oscillation is treated as an applied shear stress. The acoustic response (Δf and ΔD) of the system to this applied stress is determined. Model parameters are changed until the best fit between model and experimental Δf and ΔD values is found. The Δf and ΔD values obtained from the model are strong functions of the viscosity of the bulk fluid as well as the properties of the overlayers, including thicknesses, shear moduli, and shear viscosities.

Note that we collect Δf and ΔD at multiple harmonics. Therefore, the frequency dependence of the material properties within the film model used should be considered. The film thickness and density are frequency-independent properties. If we assume the viscoelastic properties, i.e., storage and loss moduli, are frequency-dependent, we would have up to 10 fitting parameters and only 8 data points. Therefore, we use a simple viscoelastic model for the film that imposes a particular frequency dependence on the storage and loss moduli. The Voigt and Maxwell models are the two simplest models that are able to show viscoelastic behavior. The Voigt model is usually applied to polymer systems that do not flow at a steady rate[59] and for polymer systems at high frequencies,[53] as is the case for the thin physisorbed films in this study. Thus, we use the Voigt model as the simplest system that is able to explain the data obtained.

Newtonian Liquid Model. The Δf and ΔD scaling analysis showed that the polymer systems did not demonstrate Newtonian liquid scaling pre- or postrinse. However, in the adsorption experiments, the one material property that we know changes upon the exchange of water for polymer solution is the bulk liquid viscosity. Therefore, comparing the experimental results with theoretical results for Newtonian liquids is a convenient starting point. Figure 6 compares the experimental prerinse Δf and ΔD values with the theoretical values calculated using eqs 4 and 5, where $f_1 = 4.95$ MHz, $\rho_L = 1000$ kg/m^3, and experimental bulk viscosities, $\eta_{L,exp}$, were determined using a Ubbelohde viscometer (see Table 3). For both 10 000 and 1 000 000 M_w PAs, the theory underestimates Δf and ΔD at low concentrations but overestimates them at high concentrations.

Non-Newtonian Liquid Model. Because Figure 4 shows that shear-thinning behavior can occur for these

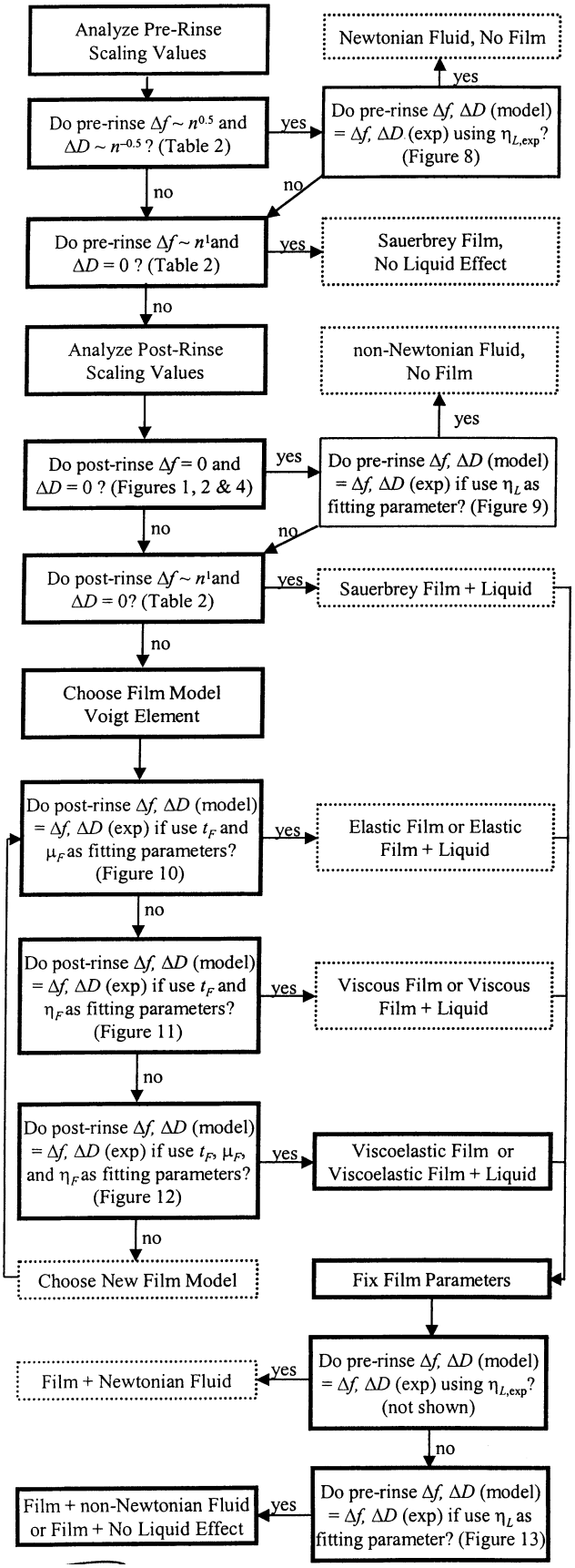

Figure 5. Flowchart of logic used in modeling the QCM-D data. Dark-outlined boxes represent the path followed through the flowchart. Light-outlined boxes represent additional steps performed as discussed in the text.

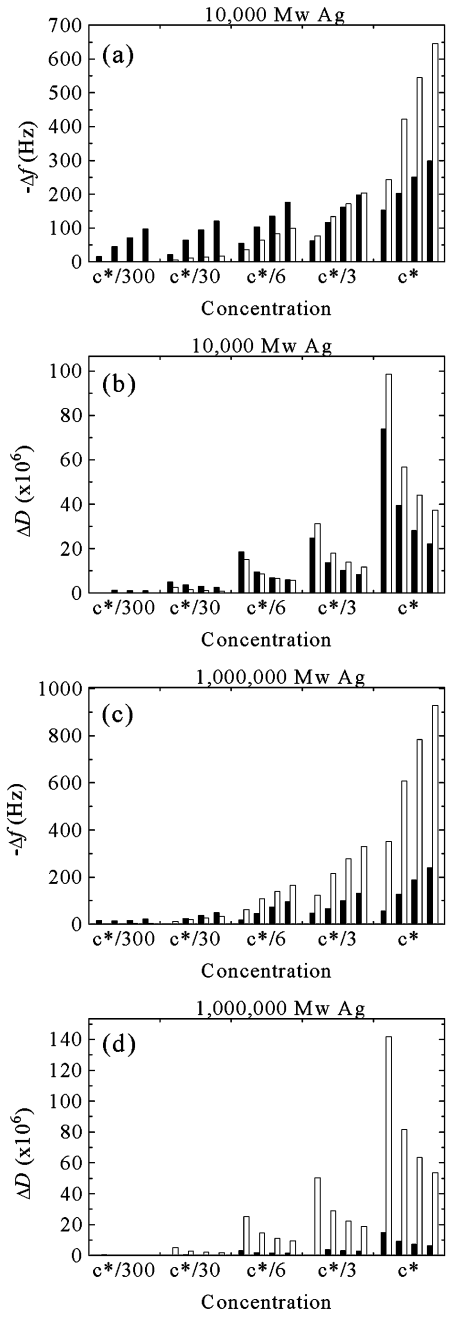

Figure 6. Comparison of experimental prerinse and Newtonian liquid theoretical Δf and ΔD values for 10 000 M_w PA on silver (a ,b) and 1 000 000 M_w PA on silver (c, d). Theoretical values are for Newtonian liquids with experimental viscosities as listed in Table 3. For each molecular weight and concentration, there are four pairs of bars. From left to right, these four pairs correspond to Δf and ΔD values at 5, 15, 25, and 35 MHz, respectively. In each pair, the solid bar on the left is the experimental value and the empty bar on the right is the theoretical value.

PA solutions, we have also allowed the liquid viscosity (η_L) to vary. Figure 7 compares the experimental prerinse Δf and ΔD values with the model. Viscosities determined in the fit are shown in Table 3. As shown, ΔD values match quite well for all concentrations and molecular weights. However, the Δf values still do not match well. Note that the prerinse β values are closer to the theoretical value for a liquid of -0.5 than the prerinse α values are to the theoretical value of 0.5. Therefore, this liquid model fits the ΔD values better

Table 3. Viscosity Values

		viscosity, η_L (10^3 Pa s)		
PA M_w/ surface	concn	exptl	non-Newtonian liquid model	viscoelastic film + non-Newtonian liquid model
10 000/Au	*c**/300	0.89	0.90	0.89
	*c**/30	0.91	0.91	0.91
	*c**/6	0.99	0.99	0.97
	*c**/3	1.11	1.08	1.04
	*c**	1.66	1.42	1.35
10 000/Ag	*c**/300	0.89	0.91	0.89
	*c**/30	0.91	0.93	0.91
	*c**/6	0.99	1.01	0.95
	*c**/3	1.11	1.06	1.01
	*c**	1.66	1.42	1.36
1 000 000/Ag	*c**/300	0.89	0.89	0.89
	*c**/30	0.92	0.90	0.89
	*c**/6	1.07	0.91	0.89
	*c**/3	1.25	0.94	0.90
	*c**	2.07	1.00	0.91

than the Δf values. For 10 000 M_w PAs, the model still underestimates Δf at low concentrations and overestimates Δf at high concentrations, while for 1 000 000 M_w PAs, Δf values are underestimated at all concentrations. As seen in Table 3, at high concentrations all of the model viscosities are significantly less than the experimental viscosities, particularly for the 1 000 000 M_w PAs.

Elastic Film Model. While the preceding system models assumed the presence of a liquid only, there is evidence for the presence of adsorbed films as well. To remove the effects of the polymer liquids on Δf and ΔD, the postrinse data are used in the modeling of the films. We assume that, after the rinsing step, we have only an adsorbed polymer film surrounded by bulk water. Also, we assume that no desorption takes place during rinsing. Since there were no changes in Δf for the 1 000 000 M_w cases during rinsing, this seems to be a reasonable assumption.

Four parameters can be used to describe the viscoelastic film in the Voigt element model: thickness (t_F), density (ρ_F), shear modulus (μ_F), and viscosity (η_F). We have between six and eight experimental data points for each case. With a larger number of fitting parameters, it is obviously easier to fit the data, but the fitting parameters can lose physical significance. Because ρ_F is not likely to vary significantly from film to film, we estimate it using other sources. The density of all films was assumed to be 1100 kg/m^3, which is comparable to densities of polyacrylamide gels.[60] We began our analysis by assuming a purely elastic film, where t_F and μ_F are allowed to vary as fitting parameters, while η_F is fixed at zero. Figure 8 compares the experimental Δf and ΔD values with those for the model. There is a tendency for the model Δf values to underestimate the experimental ones at 5 and 15 MHz, and the ΔD values do not match at all. Note that the experimental scaling is opposite to that for the model (see Figure 8b,d).

Viscous Film Model. From the previous section, we see that an elastic film model is insufficient to describe the experimental results. The other two-parameter fit is for a purely viscous film, where t_F and η_F are allowed to vary as fitting parameters, while μ_F is fixed at zero. Figure 9 compares the Δf and ΔD values for the experiment and the model. In this case, ΔD values match well for all molecular weights and concentrations. However, the model significantly underestimates Δf for almost all cases. Despite the reasonable matches for *c**/

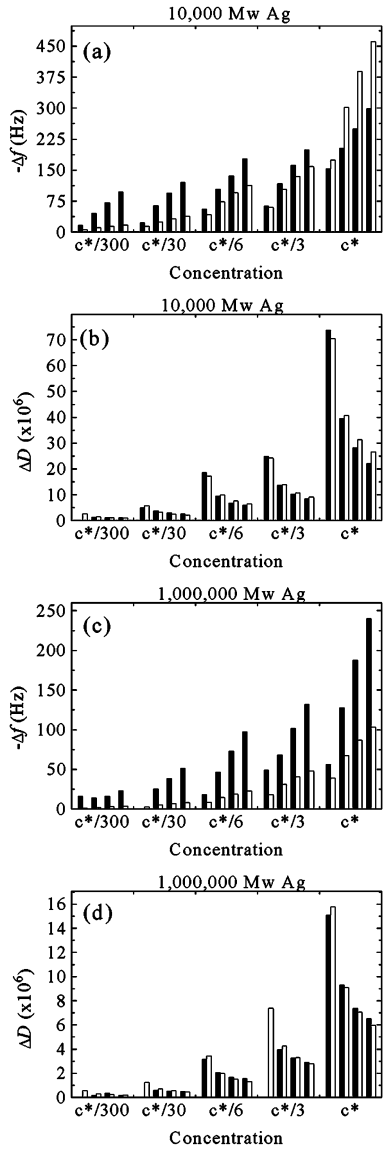

Figure 7. Comparison of experimental prerinse and non-Newtonian liquid model Δf and ΔD values for 10 000 M_w PA on silver (a, b) and 1 000 000 M_w PA on silver (c, d). η_L is allowed to vary as a fitting parameter, and no film is present in the model. The data representation is of the same form as Figure 6.

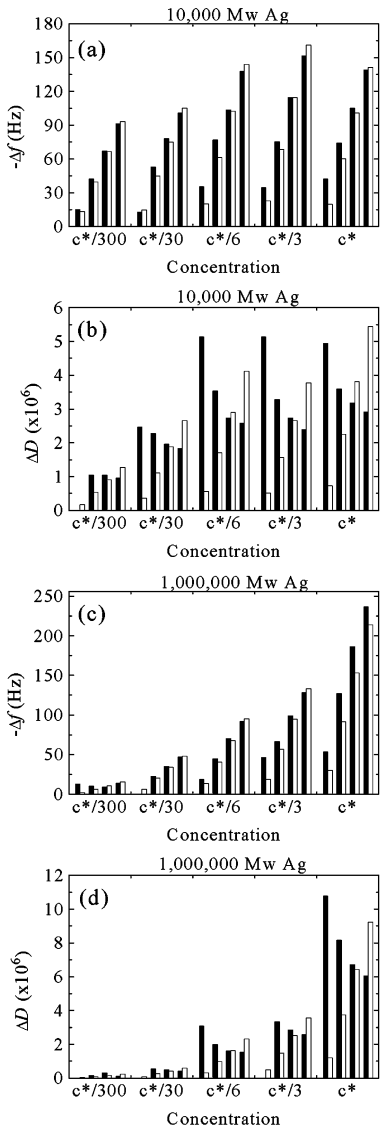

Figure 8. Comparison of experimental postrinse and elastic film model Δf and ΔD values for 10 000 M_w PA on silver (a, b) and 1 000 000 M_w PA on silver (c, d). t_F and μ_F are allowed to vary as fitting parameters. The film is assumed to be surrounded by water. The data representation is of the same form as Figure 6.

30 and $c^*/300$ solutions of 1 000 000 M_w PAs, the film properties are somewhat unreasonable. For example, the values of η_F are less than that of water itself (results not shown).

Viscoelastic Film Model. Given our inability to fit the data with only two film parameters, the next step was to use three parameters: t_F, μ_F, and η_F. Figure 10 compares the experimental Δf and ΔD values with the model values. Table 1 lists the resulting fitting parameters for each molecular weight and concentration. As shown, all Δf and ΔD values match well. The η_F values seem reasonable since they are of the same magnitude as the viscous polymer solutions. The μ_F values are comparable to those measured for bulk poly(acrylic acid) gels[61] and PA hydrogels.[62] The t_F values obtained are reasonable in that they are smaller than the size of the polymer coils, as will be discussed further in the Discussion section. Also, the t_F values obtained for the 1 000 000 M_w $c^*/30$ and $c^*/300$ PA solutions are consistent with the results of Grchev et al.[21] Finally, t_F, η_F, and μ_F are also all close to those reported for an adsorbed mussel adhesive protein (120 kDa) film in water, as determined by QCM-D.[63]

Viscoelastic Film + Non-Newtonian Liquid Model. Now that appropriate film properties have been determined using the postrinse Δf and ΔD values, we need to return to the prerinse values, where both film properties and bulk polymer solution properties contribute to Δf and ΔD. If we assume that the film properties are the same before and after the rinse, the only difference between the equilibrium and postrinse Δf and ΔD values should be caused by the presence of the viscous polymer solutions. Therefore, η_L is allowed to vary as a fitting parameter. Figure 11 compares the experimental Δf and ΔD values with the model values. Table 3 lists the η_L values determined by the model fit. For the 1 000 000 M_w PAs, the Δf and ΔD values match quite well, especially when compared to Figures 6 and 7. For the 10 000 M_w PAs the ΔD values match well. However, there are still large discrepancies between the

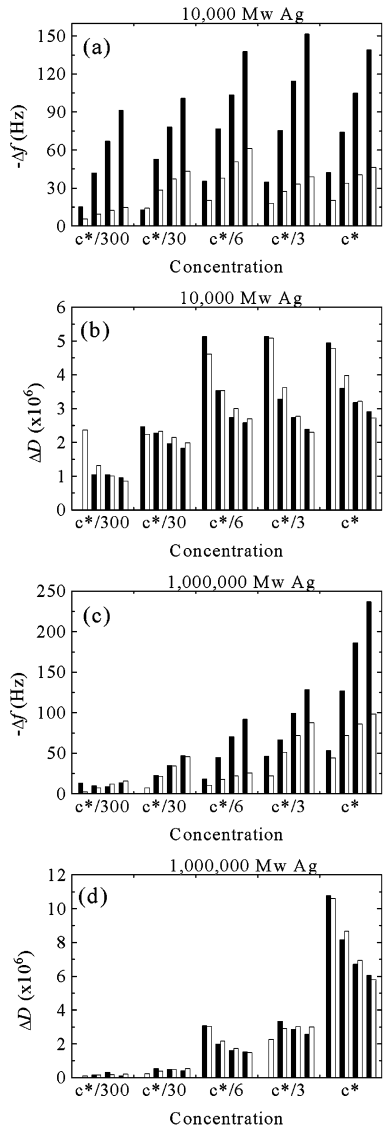

Figure 9. Comparison of experimental postrinse and viscous film model Δf and ΔD values for 10 000 M_w PA on silver (a, b) and 1 000 000 M_w PA on silver (c, d). t_F and η_F are allowed to vary as fitting parameters. The film is assumed to be surrounded by water. The data representation is of the same form as Figure 6.

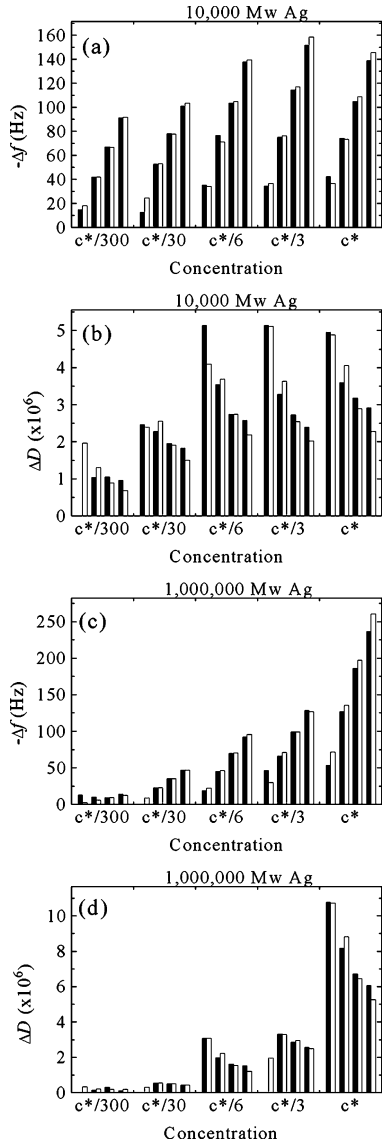

Figure 10. Comparison of experimental postrinse and viscoelastic film model Δf and ΔD values for 10 000 M_w PA on silver (a, b) and 1 000 000 M_w PA on silver (c, d). t_F, μ_F, and η_F are allowed to vary as fitting parameters. The film is assumed to be surrounded by water. The data representation is of the same form as Figure 6.

Δf values, especially at high concentrations. Moreover, the fits for c^* and $c^*/3$ solutions are no better than in Figures 6 and 7 where liquids with no films were used as the system model.

Discussion

Liquid Properties. As shown in the Rheology section, these PA solutions show non-Newtonian shear thinning behavior. Since the Carreau and Rouse models give reasonable fits to the viscosity data for PA in glycerol/water mixtures up to shear rates of 4000 s^{-1}, as shown in Figure 4, we use these models to estimate the viscosities for the PAs in water at shear rates equivalent to the operating frequency of the QCM. For this case, the viscosity of water at 25 °C, 8.9×10^{-4} Pa s, was used for η_∞ and the experimental viscosities (see Table 3) were used for η_0. Figure 12 shows the theoretical curves for 10 000 and 1 000 000 M_w c^* solutions. The 1 000 000 M_w PA solution is almost completely shear-thinned at 5 MHz. Meanwhile, the 10 000 M_w solution is just beginning to shear thin at 5 MHz. These estimates of shear-rate-dependent viscosities agree well with the viscosities determined by the fits to the data shown in Table 3. While the viscosities for the 1 000 000 M_w data are all close to the viscosity of water, the viscosities for the 10 000 M_w data are closer to the experimental solution viscosities.

This shear-thinning effect can be considered further by comparing the characteristic relaxation time of the polymer to the characteristic time of the QCM, as done by Fu et al.[64] The characteristic relaxation time of the polymer can be estimated by the Rouse time (eq 3 above). For example, for the 1 000 000 M_w c^* PA solution, $\tau_1 = 9.5 \times 10^{-5}$ s. For the 10 000 M_w c^* PA solution, $\tau_1 = 3.6 \times 10^{-8}$ s. Meanwhile, the characteristic time for the QCM—taken as the inverse of the operating frequency—at 5 MHz is 2×10^{-7} s and at 35 MHz is 2.9×10^{-8} s. Since τ_1 for the 1 000 000 M_w solution is much longer than the characteristic time of the QCM, the instrument is unable to sense the viscous effects of the

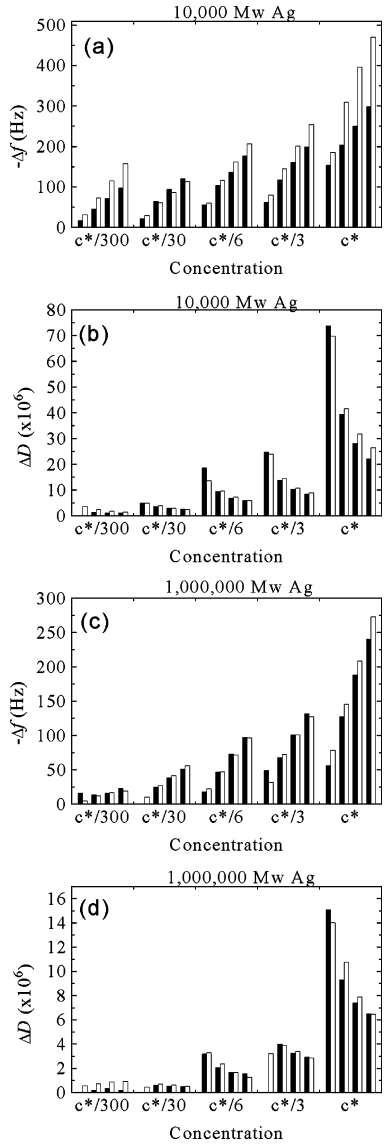

Figure 11. Comparison of experimental prerinse and viscoelastic film + non-Newtonian liquid model Δf and ΔD values for 10 000 M_w PA on silver (a, b) and 1 000 000 M_w PA on silver (c, d). Film parameters are the same as those used in Figure 10. η_L alone is allowed to vary as a fitting parameter. The data representation is of the same form as Figure 6.

solution. On the other hand, τ_1 for the 10 000 M_w solution and the characteristic time for the QCM are about equal, suggesting these bulk polymer solutions may behave viscoelastically. Our results are in excellent agreement with the theoretical treatment of non-Newtonian fluids by Nwankwo and Durning.[39]

Note that the Carreau model predicts that the viscosity of a c^* 10 000 M_w PA solution changes dramatically from 5 to 35 MHz. By contrast, all of our modeling of the QCM data has assumed frequency-independent fluid viscosities. These theoretical curves question the validity of that assumption. Unfortunately, making the fluid viscosity frequency dependent would increase the number of fitting parameters by three. A frequency-dependent liquid viscosity and the possibility of viscoelastic solution behavior may explain the discrepancies seen in the viscoelastic film + non-Newtonian liquid model for the high concentration 10 000 M_w cases. Note in Figure 11 that the model values overestimate the experimental values more at the higher harmonics

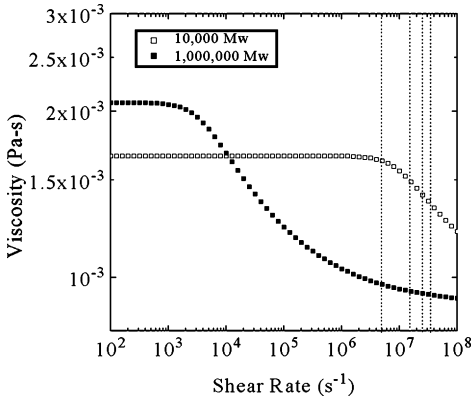

Figure 12. Theoretical shear-thinning of aqueous c^* PA solutions at high shear rates based on the Carreau and Rouse models. The vertical, dashed lines indicate the operating frequencies of the QCM: 5, 15, 25, and 35 MHz.

where, according to the Carreau theory, the viscosity of the liquid would be lower. The addition of an elastic modulus parameter for the bulk liquid might improve the fit, but that would increase the number of fitting parameters to five. Since the viscosity of the 1 000 000 M_w materials is nearly constant over the 5−35 MHz range, similar discrepancies are not seen for those cases.

Film Properties. The QTools modeling program finds the best fit by searching for a maximum in a quality factor over the parameter space. The quality factor is an inverse of the sum of errors between the experimental and model Δf and ΔD values. However, there may be a range of film properties over which reasonable fits to the data can be obtained. By using the viscoelastic model equations from the literature,[58] the ranges of η_F and μ_F values are obtained. We assume an acceptable error of ±10 Hz for each Δf value and ±1 × 10^{-6} for each ΔD value, which are similar to the variations from run to run for any given sample. The t_F values from Table 1 are not varied. Figure 13 shows the μ_F and η_F ranges for 10 000 and 1 000 000 M_w PA on silver and 10 000 M_w PA on gold. For thicker films, the size of the μ_F value range is about 40 000 Pa for a given experimental run. However, for thinner films such as c^*/30 and c^*/300 films on gold, η_F and μ_F values range over several orders of magnitude. For these thin films t_F is small compared to the acoustic decay length of the shear waves, resulting in small values of Δf and ΔD. The ranges for 1 000 000 M_w PAs are similar to those for 10 000 M_w PAs. The data obtained and model used are unable to provide more accurate property ranges for the thinner films. However, since there are no apparent trends in either η_F or μ_F values as a function of molecular weight or concentration for the thicker films, it is reasonable to assume that the properties of all the films are similar. We can establish a band of η_F and μ_F values in which at least part of the range for every experiment falls. The bounds of this band are indicated by the dashed lines in Figure 13.

The utility of QCM derives from its ability to determine the viscoelastic properties of adsorbed films. Film properties, such as thickness, density, modulus, and viscosity, are determined by the structure of the adsorbed layer. We would like to determine whether the observed trends in film properties are consistent with the concomitant structural changes suggested by theory. The well-known polymer adsorption theory developed by Scheutjens and Fleer describes polymer film structure in terms of trains, loops, and tails.[65,66] QCM should

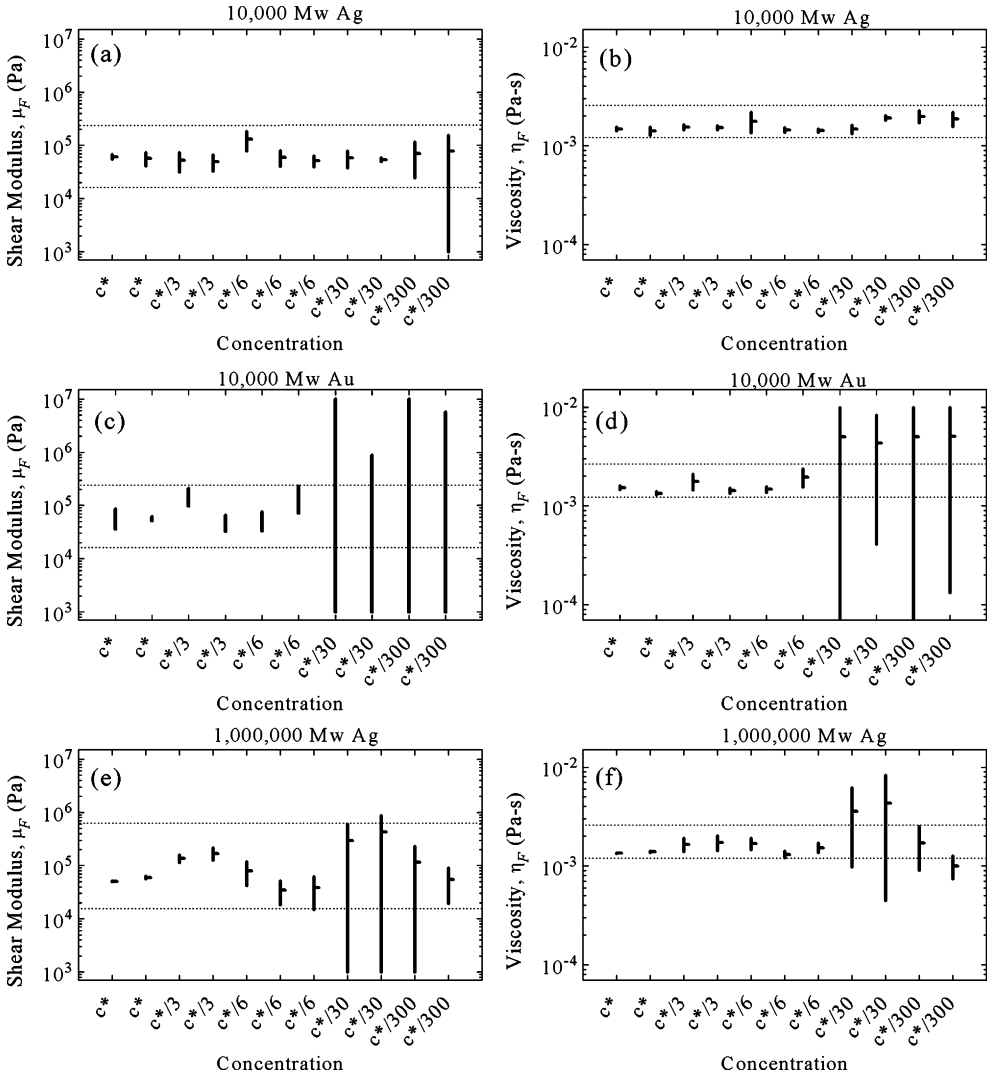

Figure 13. Film property (μ_F and η_F) ranges for 10 000 M_w PA on silver (a, b) 10 000 M_w PA on gold (c, d) and 1 000 000 M_w PA on silver (e, f). Dashed lines are at 15 000 and 228 000 Pa on modulus plots and at 1.21×10^{-3} and 2.85×10^{-3} Pa s on viscosity plots.

be sensitive to trains, loops, and tails. While only about 10% of the polymer segments are in tails for the molecular weight and concentration ranges studied here, they often extend much further from the surface than trains or loops.[66] The hydrodynamic thickness, which is determined by techniques that involve fluid flowing by adsorbed films, is sensitive to these long tails. In a QCM measurement, these tails and the fluid they entrain contribute to the frequency and dissipation response but do not dominate the measurement.

As shown in Figure 14, t_F values increase with concentration and with molecular weight, which is in accordance with both theory and numerous polymer adsorption experiments.[67] While t_F values for the 10 000 M_w PAs reach plateaus at higher concentrations, the 1 000 000 M_w material does not. Looking at the radius of gyration, R_g, of the polymer coils in solution, which can be estimated from the characteristic ratio of PA, available in the literature, we see that for 10 000 and 1 000 000 M_w PA chains in water at 25 °C, $R_g \sim 74$ and 740 Å, respectively.[47] Thus, the 10 000 M_w polymer coil is only twice as large as t_F. The polymer coils may not be able to become any more extended away from the surface, leading to a plateau in t_F. Meanwhile, for the 1 000 000 M_w materials, the t_F values are several times

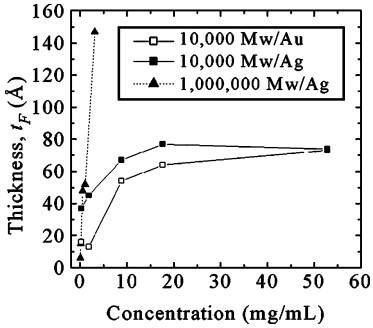

Figure 14. PA t_F values, as obtained in QCM-D viscoelastic film model, vs mass concentration.

less than the R_g values, indicating that at the highest concentrations studied there is still room for the polymer chains to extend further from the surface, such that no plateau in t_F is seen.

The modulus and viscosity parameters determined for the films depend on their structure. To draw an analogy to swollen polymer gels, basic elasticity theory states that the modulus is linearly proportional to the number of elastically active chains per unit volume. In these thin films we have polymer loops that are rigidly attached to the surface and may behave similarly to an elastic

chain segment in a network. There are also polymer tails that can contribute to the film's elasticity by forming entanglements, which act like transient cross-links.

We can use the theory of Scheutjens and Fleer to estimate the length and number of loops and tails for the molecular weight and concentration ranges studied here.[66] The molecular weight ranges over a factor of 100 and the concentration ranges over a factor of 300. According to Scheutjens and Fleer theory, a 100-fold increase in chain length would lead to, approximately, a 2-fold increase in the length of loops, a 7-fold increase in the length of tails, a 6-fold increase in the number of loops, and a less than 2-fold increase in the number of tails.[66] Similarly, a 300-fold increase in concentration would lead to, approximately, less than 2-fold increases in the length of loops or tails, a less than 2-fold decrease in the number of loops, and a less than 2-fold increase in the number of tails. Also, the fraction of segments bound to the surface in the form of trains is relatively constant over these ranges in chain length and concentration. Therefore, the length and number of loops and tails increase less than 10-fold. Meanwhile, the range of μ_F values determined from the Δf and ΔD values spans an order of magnitude. Therefore, even if the changes in number and length of loops and tails lead to large enough structural changes to affect μ_F, this suggests that the QCM would be largely unable to detect them, given the accuracy of the measurement and the model.

Surface Effects. The only apparent difference in film properties detected by the QCM for silver vs gold is t_F. As shown in Figure 14, 10 000 M_w PA films are thicker on silver than on gold, but only at low concentrations. Polyacrylamide adsorbs to gold and silver surfaces via weak coordination bonds between the nitrogen atoms of the amide groups and the metal surfaces.[68−70] These coordination bonds are known to be stronger between nitrogen and gold than between nitrogen and silver.[70] In polymer adsorption theory, the polymer surface interaction is characterized by a dimensionless adsorption energy parameter, χ_s. An increase in χ_s means stronger polymer−surface interactions, which leads to more polymer segments adsorbed to the surface. The stronger interaction of PA with gold leads to more train segments and thinner films. At higher concentrations, where there is more competition for surface sites, the difference in χ_s between silver and gold is not strong enough to result in different t_F values.

Adsorption Profile Summary. The modeling results leave us with the following picture. When polymer solution flows into the measurement chamber, there is an immediate frequency and dissipation response due to the changing liquid viscosity. Simultaneously, polymer adsorption to the surface also leads to frequency and dissipation responses. After liquid exchange is complete, polymer adsorption continues, leading to further frequency and dissipation responses. When the chamber is rinsed with water, exchanging the polymer solution for water in the measurement chamber, the frequency and dissipation again respond to the changing viscosity of the liquid. No apparent desorption takes place.

The films that are formed during adsorption are viscoelastic films with significant thicknesses. The frequency and dissipation responses observed during the adsorption process are quite dissimilar for different molecular weights. For low molecular weights, shear-thinning of the bulk fluid is just beginning to take place, such that the frequency and dissipation responses are dominated by the liquid. There is a large initial jump in Δf and ΔD due to the change in fluid viscosity that masks the formation of the polymer film on the surface. When rinsed, the large Δf and ΔD jumps are again due to the change in liquid viscosity. However, the Δf and ΔD values do not return to the baseline, indicating that a film is present on the surface. For the high molecular weight PAs, solutions are almost completely shear-thinned at the operating frequencies of the QCM. Therefore, the frequency and dissipation responses are dominated by the film. The initial jump in Δf and ΔD is due in small part to the change in the viscosity of the liquid, but in large part due to the adsorption of the film. After liquid exchange is complete, Δf and ΔD continue to change, indicating further adsorption to the surface. When rinsed, the small ΔD changes are consistent with a small change in the liquid viscosity. The lack of change in Δf indicates that no desorption is taking place and that the film properties remain constant despite the presence of a different liquid overlayer.

This picture is consistent with previous literature. Fu et al. studied the kinetics of polystyrene adsorption onto gold using the QCM.[64] When the quartz crystal was placed in polymer solution, they observed an initial jump in Δf, which they attributed to the viscosity difference between the polymer solution and pure solvent. They attributed the remainder of Δf to polymer adsorption. Discrepancies between the initial jump in Δf and Newtonian predictions of Δf changes were attributed to viscoelastic effects of bulk non-Newtonian fluids. They found that the solution behaves viscoelastically above a critical molecular weight because the critical relaxation time is of the same order as the crystal oscillation. All of the polymers studied by Fu et al. were 400 000 g/mol and above, which exceeds this critical molecular weight. Similarly, in a study of aqueous poly(ethylene glycol) solutions, Ivanchenko et al. identified changes in the dynamic viscosity of polymer solutions at high shear rates as a possible explanation for discrepancies between experiments and predictions of the frequency response for purely viscous fluids.[71] However, Ivanchenko et al. used very high concentration solutions, up to 50 wt % poly(ethylene glycol), and did not discuss adsorption of polymer chains to the surface. Finally, Xu and Schlenoff looked at polystyrene and poly(ethylene oxide) adsorption on gold from very dilute solutions.[72] Viscosity effects from such dilute solutions would only lead to a maximum change of about 5 Hz at 5 MHz.

In all three of these studies, the only data collected was the frequency change at one harmonic. By contrast, by collecting frequency and dissipation data at multiple harmonics for a wide range of molecular weights and concentrations in our work, we have been able to see the effects of the non-Newtonian liquid behavior.

Conclusions

We have studied the adsorption of PA from aqueous solutions to silver and gold surfaces as a function of molecular weight and concentration in situ using a QCM-D. In addition, we have extracted film and liquid properties from the experimental Δf and ΔD values using a viscoelastic film model. It is clear from this study that the response of the QCM-D to different molecular

weight materials can vary drastically. For the lowest molecular weight of 10 000 g/mol studied here, the Δf and ΔD responses are dominated by the viscous fluid. Meanwhile, for higher molecular weights of 500 000 and 1 000 000 g/mol, the Δf and ΔD responses are dominated by the adsorbed films, and the viscous properties of the fluids are almost undetectable. Understanding solution properties at high frequencies is critical for correct interpretation of QCM results. In addition, it is clear that when collecting QCM data over a range of frequencies, the non-Newtonian character of the bulk fluid, i.e., the frequency-dependent viscosity, must be considered.

While we have successfully extracted film properties from the QCM-D data, the precision of the property estimates is limited. The main limiting factor is t_F or, more accurately, the ΔD magnitude. In this study, for t_F values less than about 45 Å, the ΔD values are less than about 1×10^{-6}, which makes accurate fitting difficult. The number of harmonics at which data can be obtained is another limiting factor. Obviously, the more data points, the more accurate the fit to the data. For the films studied here, t_F increases with both molecular weight and concentration. However, μ_F and η_F values are relatively constant, independent of the molecular weight or concentration of the PA solution. In addition, large property ranges can describe a single film. This makes it difficult to determine whether any structural differences exist between the adsorbed films. Determining the viscoelastic properties of such thin films may help determine the appropriate molecular weight and concentration ranges for adsorption as well as help to identify polymers that will be useful for a specific application.

Acknowledgment. We thank Kay Kanazawa for his comments and suggestions on the QCM-D analysis. Financial support for the project was provided by a NSF Graduate Research Fellowship (J.C.M.), the NSF XYZ-on-a-chip program under DMR-9980799, and the Center on Polymer Interfaces and Macromolecular Assemblies (CPIMA), which is sponsored by the NSF-MRSEC program under DMR-9808677.

References and Notes

(1) Tamm, L. K.; McConnell, H. M. *Biophys. J.* **1985**, *47*, 105−113.
(2) Koenig, B. W.; Krueger, S.; Orts, W. J.; Majkrzak, C. F.; Berk, N. F.; Silverton, J. V.; Gawrisch, K. *Langmuir* **1996**, *12*, 1343−1350.
(3) Bayerl, T. M.; Bloom, M. *Biophys. J.* **1990**, *58*, 357−362.
(4) Johnson, S. J.; Bayerl, T. M.; McDermott, D. C.; Adam, G. W.; Rennie, A. R.; Thomas, R. K.; Sackmann, E. *Biophys. J.* **1991**, *59*, 289−294.
(5) Poglitsch, C. L.; Sumner, M. T.; Thompson, N. L. *Biochemistry* **1991**, *30*, 6662−6671.
(6) Hinterdorfer, P.; Baber, G.; Tamm, L. K. *J. Biol. Chem.* **1994**, *269*, 20360−20368.
(7) Salafsky, J.; Groves, J. T.; Boxer, S. G. *Biochemistry* **1996**, *35*, 14773−14781.
(8) Sackmann, E. *Science* **1996**, *271*, 43−48.
(9) Majewski, J.; Wong, J. Y.; Park, C. K.; Seitz, M.; Israelachvili, J. N.; Smith, G. S. *Biophys. J.* **1998**, *75*, 2363−2367.
(10) Wong, J. Y.; Majewski, J.; Seitz, M.; Park, C. K.; Israelachvili, J. N.; Smith, G. S. *Biophys. J.* **1999**, *77*, 1445−1457.
(11) Wong, J. Y.; Park, C. K.; Seitz, M.; Israelachvili, J. *Biophys. J.* **1999**, *77*, 1458−1468.
(12) Luo, G. B.; Liu, T. T.; Zhao, X. S.; Huang, Y. Y.; Huang, C. H.; Cao, W. X. *Langmuir* **2001**, *17*, 4074−4080.
(13) Kuhner, M.; Tampe, R.; Sackmann, E. *Biophys. J.* **1994**, *67*, 217−226.
(14) Dietrich, C.; Tampe, R. *Biochim. Biophys. Acta* **1995**, *1238*, 183−191.
(15) Elender, G.; Kuhner, M.; Sackmann, E. *Biosens. Bioelectron.* **1996**, *11*, 565−577.
(16) Spinke, J.; Yang, J.; Wolf, H.; Liley, M.; Ringsdorf, H.; Knoll, W. *Biophys. J.* **1992**, *63*, 1667−1671.
(17) Wagner, M. L.; Tamm, L. K. *Biophys. J.* **2000**, *79*, 1400−1414.
(18) Shen, W. W.; Boxer, S. G.; Knoll, W.; Frank, C. W. *Biomacromolecules* **2001**, *2*, 70−79.
(19) Munro, J. C.; Frank, C. W. *Polymer* **2003**, *44*, 6335−6344.
(20) Grchev, T.; Cvetkovska, M.; Schultze, J. W. *Corros. Sci.* **1991**, *32*, 103−112.
(21) Grchev, T.; Cvetkovska, M.; Stafilov, T.; Schultze, J. W. *Electrochim. Acta* **1991**, *36*, 1315−1323.
(22) Pefferkorn, E.; Carroy, A.; Varoqui, R. *Macromolecules* **1985**, *18*, 2252−2258.
(23) Parsonage, E.; Tirrell, M.; Watanabe, H.; Nuzzo, R. G. *Macromolecules* **1991**, *24*, 1987−1995.
(24) Frantz, P.; Granick, S. *Langmuir* **1992**, *8*, 1176−1182.
(25) Malmsten, M.; Lindman, B. *Langmuir* **1990**, *6*, 357−364.
(26) Advincula, R.; Aust, E.; Meyer, W.; Knoll, W. *Langmuir* **1996**, *12*, 3536−3540.
(27) *Applications of Piezoelectric Quartz Crystal Microbalances*; Lu, C., Czanderna, A. W., Eds.; Elsevier: New York, 1984; Methods and Phenomena Series, Vol. 7.
(28) Sauerbrey, G. *Z. Phys.* **1959**, *155*, 206−222.
(29) Nomura, T.; Minemura, A. *Nippon Kagaku Kaishi* **1980**, 1621−1625.
(30) Buttry, D. A.; Ward, M. D. *Chem. Rev.* **1992**, *92*, 1355−1379.
(31) Rodahl, M.; Kasemo, B. *Rev. Sci. Instrum.* **1996**, *67*, 3238−3241.
(32) Geelhood, S. J.; Frank, C. W.; Kanazawa, K. *J. Electrochem. Soc.* **2002**, *149*, H33−H38.
(33) Kanazawa, K. K.; Gordon, J. G. *Anal. Chem.* **1985**, *57*, 1770−1771.
(34) Kanazawa, K. K.; Gordon, J. G. *Anal. Chim. Acta* **1985**, *175*, 99−105.
(35) Miller, J. G.; Bolef, D. I. *J. Appl. Phys.* **1968**, *39*, 4589−4593.
(36) Benes, E. *J. Appl. Phys.* **1984**, *56*, 608−626.
(37) Nowotny, H.; Benes, E. *J. Acoust. Soc. Am.* **1987**, *82*, 513−521.
(38) Kanazawa, K. K.; Melroy, O. R. *IBM J. Res. Dev.* **1993**, *37*, 157−171.
(39) Nwankwo, E.; Durning, C. J. *Rev. Sci. Instrum.* **1998**, *69*, 2375−2384.
(40) Bandey, H. L.; Martin, S. J.; Cernosek, R. W.; Hillman, A. R. *Anal. Chem.* **1999**, *71*, 2205−2214.
(41) White, C. C.; Schrag, J. L. *J. Chem. Phys.* **1999**, *111*, 11192−11206.
(42) Johannsmann, D.; Mathauer, K.; Wegner, G.; Knoll, W. *Phys. Rev. B: Condens. Matter* **1992**, *46*, 7808−7815.
(43) Bandey, H. L.; Hillman, A. R.; Brown, M. J.; Martin, S. J. *Faraday Discuss.* **1997**, *107*, 105−121.
(44) Brown, M. J.; Hillman, A. R.; Martin, S. J.; Cernosek, R. W.; Bandey, H. L. *J. Mater. Chem.* **2000**, *10*, 115−126.
(45) Hillman, A. R.; Jackson, A.; Martin, S. J. *Anal. Chem.* **2001**, *73*, 540−549.
(46) Domack, A.; Prucker, O.; Ruhe, J.; Johannsmann, D. *Phys. Rev. E* **1997**, *56*, 680−689.
(47) Orwoll, R. A.; Chong, Y. S. In *Polymer Data Handbook*; Mark, J. E., Ed.; Oxford University Press: New York, 1999; pp 247−251.
(48) Lide, D. R. *CRC Handbook of Chemistry and Physics*, 75th ed.; CRC Press: Boca Raton, FL, 1994.
(49) Rodahl, M.; Hook, F.; Krozer, A.; Brzezinski, P.; Kasemo, B. *Rev. Sci. Instrum.* **1995**, *66*, 3924−3930.
(50) Ron, H.; Rubinstein, I. *Langmuir* **1994**, *10*, 4566−4573.
(51) Vlassopoulos, D.; Schowalter, W. R. *J. Rheol.* **1994**, *38*, 1427−1446.
(52) Lopez, F. V.; Pauchard, L.; Rosen, M.; Rabaud, M. *J. Non-Newtonian Fluid Mech.* **2002**, *103*, 123−139.
(53) Barnes, H. A. *A Handbook of Elementary Rheology*; University of Wales Institute of Non-Newtonian Fluid Mechanics: Aberystwyth, Wales, 2000.
(54) Bottom, V. E. *Introduction to Quartz Crystal Unit Design*; Van Nostrand Reinhold Co.: New York, 1982.
(55) Rodahl, M.; Kasemo, B. *Sens. Actuators, A* **1996**, *54*, 448−456.
(56) Stockbridge, C. D. In *Vacuum Microbalance Techniques*; Katz, M. J., Ed.; Plenum Press: New York, 1966; Vol. 5, pp 147−178.
(57) Rodahl, M.; Hook, F.; Fredriksson, C.; Keller, C. A.; Krozer, A.; Brzezinski, P.; Voinova, M.; Kasemo, B. *Faraday Discuss.* **1997**, *107*, 229−246.

(58) Voinova, M. V.; Rodahl, M.; Jonson, M.; Kasemo, B. *Phys. Scr.* **1999**, *59*, 391−396.
(59) Philippoff, W. In *Physical Acoustics*; Mason, W. P., Ed.; Academic Press: New York, 1965; Vol. 2B, pp 1−90.
(60) Hirata, Y.; Kato, Y.; Andoh, N.; Fujiwara, N.; Ito, R. *J. Chem. Eng. Jpn.* **1993**, *26*, 143−147.
(61) Schosseler, F.; Ilmain, F.; Candau, S. J. *Macromolecules* **1991**, *24*, 225−234.
(62) Dubrovskii, S. A.; Rakova, G. V. *Macromolecules* **1997**, *30*, 7478−7486.
(63) Hook, F.; Kasemo, B.; Nylander, T.; Fant, C.; Sott, K.; Elwing, H. *Anal. Chem.* **2001**, *73*, 5796−5804.
(64) Fu, T. Z.; Stimming, U.; Durning, C. J. *Macromolecules* **1993**, *26*, 3271−3281.
(65) Scheutjens, J. M. H. M.; Fleer, G. J. *J. Phys. Chem.* **1979**, *83*, 1619−1635.
(66) Scheutjens, J. M. H. M.; Fleer, G. J. *J. Phys. Chem.* **1980**, *84*, 178−190.
(67) Fleer, G. J.; Cohen Stuart, M. A.; Scheutjens, J. M. H. M.; Cosgrove, T.; Vincent, B. *Polymers at Interfaces*; Chapman & Hall: New York, 1993.
(68) Bharathi, S.; Fishelson, N.; Lev, O. *Langmuir* **1999**, *15*, 1929−1937.
(69) Ooka, A. A.; Kuhar, K. A.; Cho, N. J.; Garrell, R. L. *Biospectroscopy* **1999**, *5*, 9−17.
(70) Michota, A.; Kudelski, A.; Bukowska, J. *Surf. Sci.* **2002**, *502*−*503*, 214−218.
(71) Ivanchenko, M. I.; Kobayashi, H.; Eduard, A. K.; Dobrova, N. B. *Anal. Chim. Acta* **1995**, *314*, 23−31.
(72) Xu, H.; Schlenoff, J. B. *Langmuir* **1994**, *10*, 241−245.

MA030297W